Novel Mechanisms for Advanced Propulsion Systems

Madhusudan Raghavan

Abstract

This paper presents two interesting mechanisms-related problems in the area of advanced propulsion systems, one in power generation and the other in power transmission. The first is an opposed-piston variable compression ratio engine mechanism for possible use in advanced powertrains. The concept is a two-stroke engine equipped with a Roots supercharger to facilitate the scavenging process. The engine has been numerically evaluated using 1-D and 3-D simulation tools. We present the kinematic details of the mechanism arrangement that serves to couple the two cranks which may be selectively phased relative to each other to achieve a variable compression ratio. Secondly, the paper describes a high-speed flywheel system and its use as an alternative energy storage system for recapturing vehicle kinetic energy as a low-cost hybrid architecture. Such a system has the potential to improve fuel economy by 15-20% on the certification drive-cycle when coupled to the driveline via a three-speed clutched transmission system in a representative mid-size vehicle. The fuel economy gain is shown to be due to idle stop/start, recuperation of vehicle kinetic energy during deceleration events, launching of the vehicle with the flywheel, and driveline torque boosting to offset fuel use. We present simulation results on drive cycle fuel consumption as well as the kinematic details of the geared arrangement to get energy into and out of the flywheel system.

Keywords: variable compression ratio, opposed piston, flywheel hybrid, three-speed coupling

1 Introduction

The 2013 International Energy Outlook [1] offers the following forecasts regarding population growth and energy consumption in the future. Global population grows 28% from 6.9 billion in 2010 to 8.8 billion in 2040. Population remains concentrated in Asia and Africa. Their share of the global population is 70% in 2010 and 72% in 2040. China's population peaks in 2025. Most other regions continue to grow through 2040, but their rate of growth slows. Real GDP rises by an average of 3.6% per year globally from 2010 to 2040. Projected values range from a high of 5.7% for China to a low of 0.7% for the Middle East. Total world marketed energy will grow by 56% from 2010 to 2040, from 524 quads to 820 quads (quad = quadrillion Btu) with transportation sector projected usage shown in Figure 1. A strong demand growth in non-OECD (Organization for Economic Cooperation and Development) countries of 90% is driven by higher long-term economic growth rates. OECD fuel economy standards for vehicles will likely be adopted throughout the world and will moderate future growth in liquid fuels consumption. Fuel economy standards and high oil prices will cause petroleum's share of world energy to fall from 33% in 2010 to 28% in 2040. Worldwide energy-related CO2 emissions will rise from about 31 billion metric tons in 2010 to 45 billion metric tons in 2040, a 46% increase. A steady growth of

Madhusudan Raghavan
GM R&D Center, Warren, Michigan, USA, E-mail:madhu.raghavan@gm.com.

urbanization will increase the standard of living and drive the demand for efficient personal transportation vehicles.

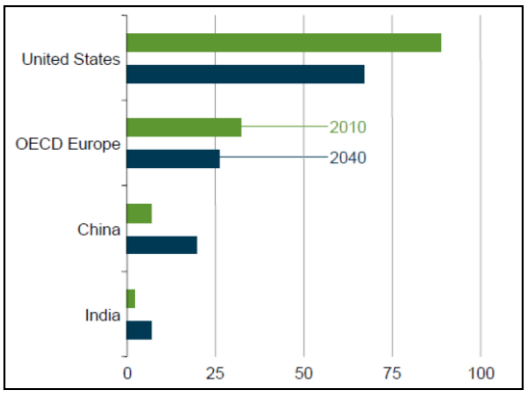

Figure 1: Transportation Sector per Capita Energy Use (MMBtu)

Against this backdrop of increasing population, energy consumption, urbanization, congestion and pollution, we are looking at ways to improve vehicle fuel economy by minimizing engine fuel consumption and hybridization of the driveline as proposed in the subsequent sections of this paper.

2 Background and Prior Art

We briefly review some recent offerings in the advanced powertrain literature. Robinette and Powell [2] describe the use of a 12V start/stop system to turn the engine off and on during periods of vehicle idle. In particular integration issues such as start ability, noise and vibration, and vehicle launch are discussed in addition to the use of a correlated lump parameter modeling methodology. Hawkins et al. [3] describe General Motors' eAssist powertrain, which delivers approximately three times the peak electric boost and regenerative braking capability of GM's first generation 36V BAS. Key elements include a water-cooled induction motor/generator, an accessory drive with a coupled dual tensioner system, air cooled power electronics integrated with a 115V lithium-ion battery pack, a direct-injection 2.4 liter 4-cylinder gasoline engine, and a modified 6-speed automatic transmission.

An example of a highly successful electrically variable transmission (EVT) concept developed at GM is the two-mode hybrid system produced for transit buses and SUVs. Schmidt [4] describes an embodiment with three planetary gear sets coaxially aligned. Gear members of the first and second planetary gear set are respectively connected to the two motor/generators. Their carriers are operatively connected to the output member. The two-mode system innovations provide performance and fuel economy improvements at highway speeds and better trailer towing ability. Grewe et al [5] describe the General Motors 2-Mode Hybrid transmission for full-size, full-utility SUVs. This system integrates two electromechanical power-split operating modes

with four fixed gear ratios and provides fuel savings from electric assist, regenerative braking and low-speed electric vehicle operation.

Miller et al. [6] describe the Voltec 4ET50 multi-mode electric transaxle, which introduces a unique two-motor EV driving mode that allows both the driving motor and the generator to simultaneously provide tractive effort while reducing electric motor speeds and the total associated electric motor losses. This new operating mode, however, does not introduce the torque discontinuities associated with a two-speed EV drive. For extended range operation, the Voltec transaxle provides both the completely decoupled action of a pure series hybrid, as well as a more efficient powerflow with decoupled action for driving at light loads and high vehicle speed. Additionally, Conlon et al. [7] describe the improvements made in the 2nd generation design of the Volt drivetrain, as a result of which, the vehicle is projected to achieve a 30% increase in EV range, an 11% improvement in charge sustaining label fuel economy, and improved vehicle performance both as an electric vehicle, and in extended range mode.

Raghavan, Chanumolu and Park [8] describe a novel propulsion architecture and a novel charging system for urban vehicles. The novel parallel hybrid configuration consists of a DC hub motor coupled to an IC engine. This configuration adds speed to the wheel output; the addition of speed does not require a complex transmission and may be achieved by simply connecting the output of the IC engine to the stator of an electric hub motor. The study of this "city car" concept is extended beyond the propulsion system and also explores convenient recharging of the onboard battery via a prototype "hands free" robotic conductive charging device for ease of use. The key research results presented in this context, include a localization algorithm for determining the location of the plug-in receptacle, using low-cost RFID technology.

Raghavan [9] discusses alternative propulsion architectures with mechanical energy storage and evaluates them from the standpoint of efficiency and potential for use in automobiles. He studies air hybrids and describes modelling and simulation results along with experimental data from a test-bed to assess round-trip efficiencies of such storage systems. This is followed by an assessment of hydraulic hybrids and flywheel hybrids. These systems are sized for comparable applications. Simulations are then used to objectively compare losses in these systems and to estimate operating round-trip efficiencies in energy storage applications.

3 Significance of the Present Work

This paper presents two mechanisms-related challenges in the area of advanced propulsion systems, one in power generation and the other in power transmission. The first is an opposed-piston variable compression ratio engine mechanism for possible use in advanced powertrains. The concept is a two-stroke engine equipped with a Roots supercharger to facilitate the scavenging process. The engine has been numerically evaluated using 1-D and 3-D simulation tools. We present the kinematic details of the mechanism arrangement that serves to couple the two cranks which may be selectively phased relative to each other to achieve a variable compression ratio. Secondly, the paper describes a high-speed flywheel system and its use as an alternative energy storage system for recapturing vehicle kinetic energy as a low-cost hybrid architecture. Such a system has the potential to improve fuel economy by 15-

20% on the certification drive-cycle when coupled to the driveline via a three-speed clutched transmission system in a representative mid-size vehicle. The fuel economy gain is shown to be due to idle stop/start, recuperation of vehicle kinetic energy during deceleration events, launching of the vehicle with the flywheel, and driveline torque boosting to offset fuel use. We present simulation results on drive cycle fuel consumption as well as the kinematic details of the geared arrangement to get energy into and out of the flywheel system.

4 Powertrain Mechanism Concept 1

The opposed piston engine concept, shown in Fig. 2 was conceived at GM R&D by Maguire et al. [10] and its combustion design, modeling and simulation were conducted by our research collaborators, Prof. Ingemar Denbratt and his colleagues at Chalmers University. The engine has pairs of cylinders that are placed in-line, head to head. There is no cylinder head; the clearance volume when the piston is at the top of its stroke is effectively the gap between the tops of the respective pairs of pistons. There are two crankshafts which are coupled mechanically via a gear train as shown in Fig. 2. This gear train effectively converts this two crankshaft system into a single crankshaft system and we may use either crankshaft as the engine output depending on vehicle architecture and packaging convenience.

Subsequent analysis showed that one could achieve additional engine efficiency improvements by introducing a single degree-of-freedom control input in this mechanical coupling, which allows the crankshafts to be phased relative to one another. This phase change modifies the compression ratio by changing the clearance volume by appropriately phasing the piston motions. An embodiment of this adjustable mechanical coupling between the two crankshafts is a planetary gear set and a pair of sprockets and chains connecting the components of the gear set to the two crankshafts (see Fig. 3). The shaft on the left (crank 1) is connected to the ring gear of the planetary set, and the shaft on the right (crank 2) is connected to the carrier of the planetary gear set.

Kinematic and dynamic simulations of this embodment of the opposed piston engine were conducted within GM R&D's Hybrid Systems group by Nagini Devarakonda, and are described in the following sections. The focus of this work was on the design of the phaser mechanism coupling the 2 cranks. This engine was designed to operate on a 2-stroke cycle. Power and exhaust cycles in one cylinder are accompanied by the intake and compression strokes in the other cylinder. Each crankshaft is driven by the

pistons on the corresponding side. In the simulations, a planetary gear set with a ring-to-sun ratio of 2.0 was considered.

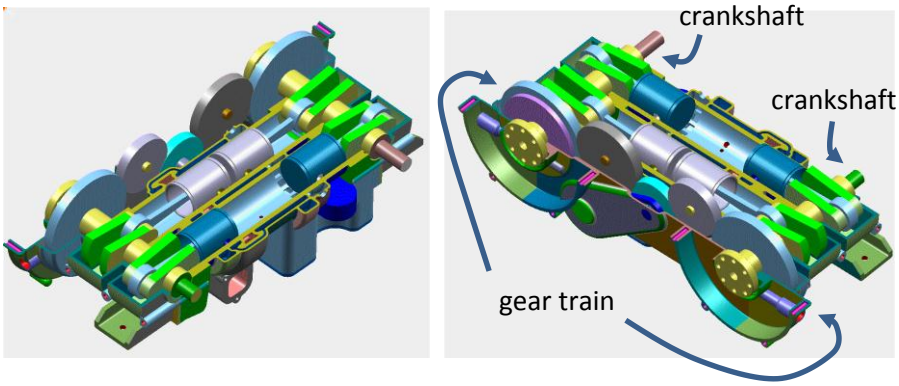

Figure 2: Opposed Piston Engine Concept

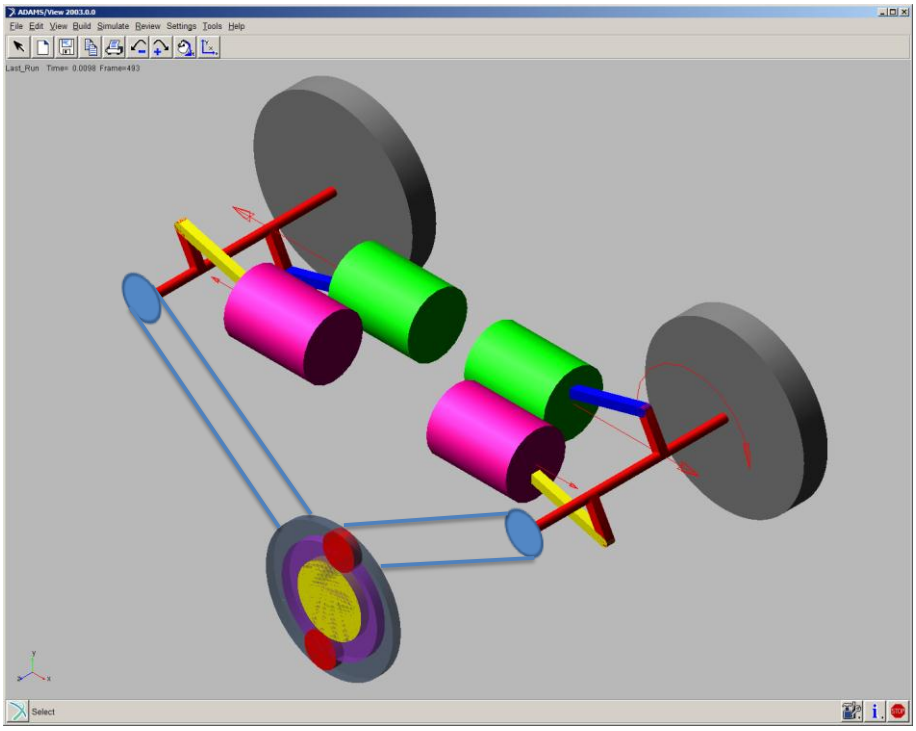

Figure 3: Planetary Gear Set with Chains to Crankshafts

4.1 Simulation

In order to simulate the kinematics of the engine, the force produced by combustion was modeled. Cylinder pressure as a function of Crank Angle Degree (CAD) was available from GT-Power simulations and from this data, the force produced by combustion (as a function of pressure) was calculated and appears as shown in Fig. 4. In the simulation, the force was derived from a look up table as a function of the distance between the two pistons. The modeled force was used to simulate the combustion in both the cylinders with the proper phase difference. Forces at the bearings supporting the crankshafts, as well as the velocities and the displacements at various joints were recorded as functions of time.

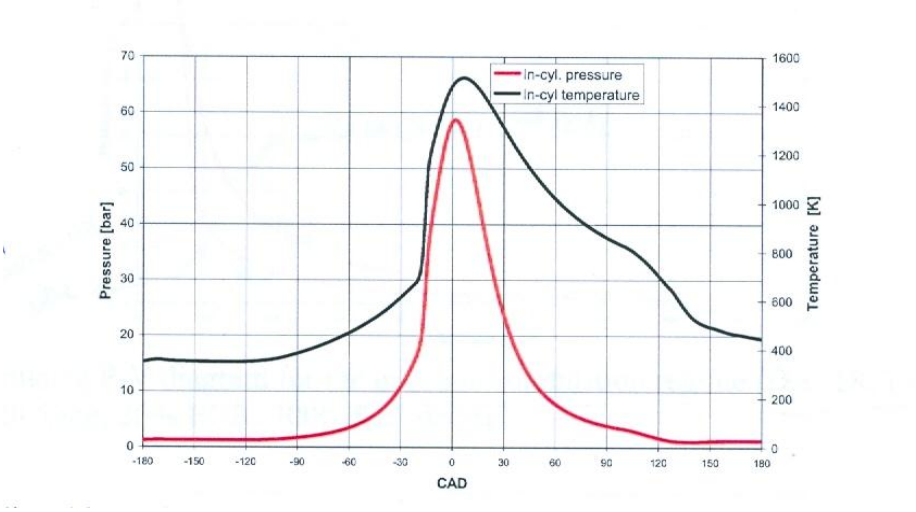

Figure 4: Estimate of Force due to Combustion

4.2 Results

One of the objectives of the phaser simulation was to calculate the torques and the forces acting on each component, particularly the sun gear. This was done in order to size the actuating device such as an electric motor. Fig. 5 shows forces and torques during a phase change maneuver. The sharp increase in the torque at the sun gear is mainly due to the inertial loading. It should be noted that the phaser planetary-gear ratio here is 2.0, and a harmonic drive phaser with a much larger ratio would result in lower torques on the actuation device. Also seen in this figure are the periodic gas forces in the cylinders with a constant phase difference.

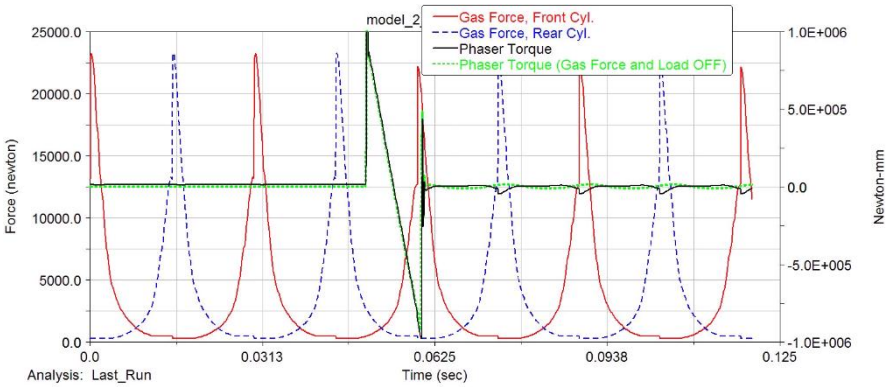

Figure 5: Torque at Sun Gear During Phase Change Maneuver

This phase change between the pairs of pistons will impact the port timing as the intake and exhaust events are controlled by moving pistons clearing the ports near the bottom-dead-center position. Fig. 6 shows the change in the compression ratio and piston-piston distance as a function of the phase angle (the rotation of the sun gear relative to ground).

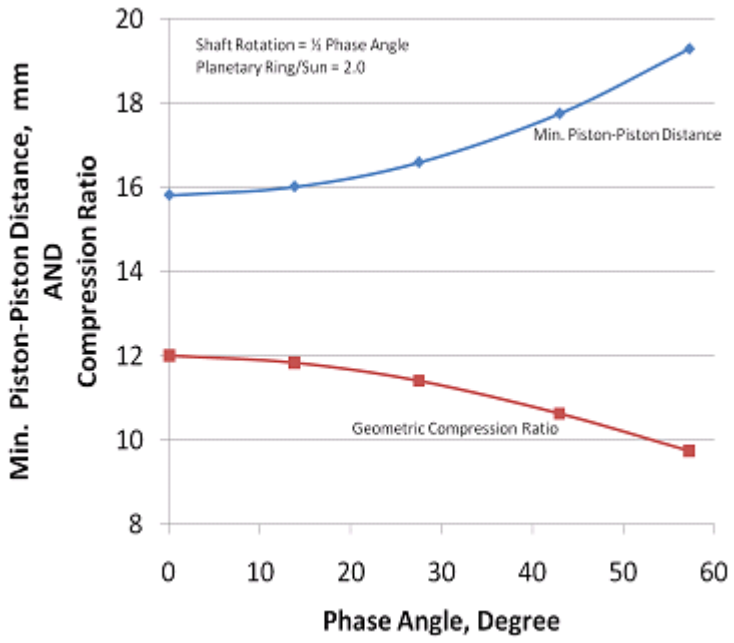

Figure 6: Variation in Compression Ratio and Minimum Piston-Piston Distance

5 Powertrain Mechanism Concept 2

Recent developments in flywheel technology have made it a credible alternative energy storage system (ESS) for hybrid vehicles [11], [12]. The advantages of flywheel systems include high power density, durability, potentially lower material cost, and the elimination of energy conversion between the mechanical and electrical domains. The analysis described in the subsequent sections was conducted by Dongsuk Kum and Norman Bucknor of GM R&D's Hybrid Systems group in partnership with our research collaborators, Flybrid Systems LLC, of UK.

The way a high-speed flywheel system works is it recuperates vehicle kinetic energy that would normally be lost through braking and launches/propels the vehicle with this stored energy. This simple recuperation-launch strategy allows the engine to shut-down during braking, stop, and launch, when the engine operates in its inefficient regions. For energy storage applications, the flywheel and its auxiliary components need to be designed to operate at high speed because the kinetic energy KE_f, stored by a flywheel is proportional to the flywheel rotational speed squared, whereas it is proportional to the flywheel inertia as Eq. (1) shows.

$$KE_f = \frac{1}{2} I_f {\omega_f}^2 \tag{1}$$

where I_f is the flywheel inertia, and ω_f is the flywheel rotational speed. Also, note that the amount of stored energy, also known as the state-of-charge (SOC), can be easily and accurately computed from the rotational speed as follows.

$$SOC = \frac{KE_f}{KE_{max}} = \frac{{\omega_f}^2}{{\omega_{f,max}}^2} \tag{2}$$

where $\omega_{f,max}$ is predetermined by the flywheel design.

Flywheel kinetic energy recovery systems (KERS) can be used in many different hybrid powertrain configurations. In this study, a post-transmission configuration (shown in Fig. 7(b)) is chosen mainly due to its practical advantages such as packaging, cost, and minimal design changes from the conventional vehicle. Figure 7 shows that both the engine and flywheel have dedicated transmissions, which allows the engine to operate independent of the flywheel speed as well as the vehicle speed. A conventional automatic transmission and a torque converter are used for the engine, and a clutch flywheel transmission (CFT) is used for the flywheel.

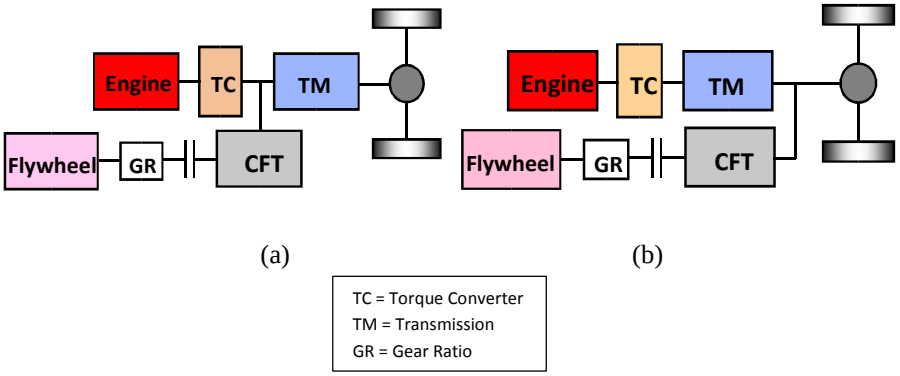

Figure 7: Schematic of the (a) pre-transmission and (b) post-transmission flywheel hybrid powertrain configuration

5.1 Modeling of Flywheel Hybrid Drivetrain

A Simulink HEV model was developed based on the schematic in Fig. 7(b). The model consists of a conventional driveline, flywheel driveline, and a supervisory controller. The conventional driveline includes an engine, torque converter, and a conventional automatic transmission, and the flywheel driveline includes the flywheel dynamics and the CFT. The supervisory controller coordinates two power sources, the engine and the flywheel, depending on the vehicle state and driver demand.

The target vehicle is a generic mid-size vehicle with a 1.8L SI engine and a 6-speed automatic transmission. Table 1 shows that the flywheel hybrid vehicle shares all of

Table 1: Vehicle Parameters

		Conventional vehicle	Flywheel hybrid vehicle
Mass		1530kg	1580kg
1.8L SI Engine		103kw (138hp) @6300rpm	
		167Nm (123lbft) @3800rpm	
Automatic Transmission		6 speed [4.449 2.908 1.893 1.446 1 0.742]	
Final Drive		3.94:1	
CFT	Gear Ratio	N/A	[4.847 2.915 1.667]
	3-Stage Gear		6.44:1
Flywheel	Inertia	N/A	0.014 kgm^2
	Capacity		76.8 Wh (276 kJ)
CFT + Flywheel Mass			50kg

the conventional vehicle's driveline components. The CFT has three clutches with different gear ratios across them, and it has a three-stage speed reduction gear connecting the CFT output to the automatic transmission output shaft. The flywheel inertia is quite small and can store 76.8Wh (276kJ) at the maximum operating speed of 60,000 rpm.

The engine speed dynamics is described by a simple rotational dynamics model, and the fuel consumption is computed based on the throttle input and the engine speed.

$$\frac{d\omega_{eng}}{dt} = \frac{T_{eng} - T_{aux} - T_{TC}}{J_{eng}}, \text{where } T_{eng} = f(\theta, \omega_{eng}),\ T_{aux} = f(\theta, \omega_{eng}) \tag{3}$$

$$\frac{dFC}{dt} = f(\theta, \omega_{eng}) \tag{4}$$

where ω_{eng} is engine speed, FC is the fuel consumption, T_{eng} is engine torque, T_{aux} is auxiliary loss, T_{TC} is reaction torque from the torque converter, θ is the throttle input, J_{eng} is the engine inertia. Engine torque and fuel consumption rates are calculated using quasi-static maps. Fast dynamics such as intake manifold dynamics are assumed to have negligible influence on the model. The K-factor modeling approach is used to compute the transmission input torque and the turbine reaction torque of the torque converter.

$$T_{turbine} = \left(\frac{\omega_{eng}}{K_{factor}(SR)}\right)^2, \tag{5}$$

where $SR = \frac{\omega_{eng}}{\omega_{i,TM}}$ and $\omega_{i,TM}$ is transmission input shaft speed

A quasi-static model is used for the transmission. Transmission output torque is computed as follows.

$$T_{o,TM} = \begin{cases} \eta_{GR} GR \cdot T_{i,TM} - C_{TM}\omega_{i,TM}, & \text{for } T_{i,TM} \geq 0 \\ \dfrac{GR \cdot T_{i,TM}}{\eta_{GR}} - C_{TM}\omega_{i,TM}, & \text{for } T_{i,TM} < 0 \end{cases} \tag{6}$$

where $T_{o,TM}$ is output transmission torque, η_{GR} = gear efficiency, GR is gear ratio, C_{TM} is spin (viscous) loss coefficient. $\omega_{i,TM}$, the transmission input shaft speed is computed as follows.

$$\omega_{i,TM} = GR \cdot \omega_{o,TM} \tag{7}$$

The longitudinal vehicle dynamics is described by various forces acting on a lumped mass

$$\frac{dV}{dt} = \frac{F_D - F_B - F_R}{M_r}, \text{where } F_R = f_0 + f_1 V + f_2 V^2$$

$$\text{and } T_{sum} = T_{o,TM} + T_{o,CFT} \tag{8}$$

where V is vehicle speed, F_D is the tractive force, F_B is the braking force, F_R is the road load, T_{sum} is the summation of two torques applied at the final drive, and $T_{o,CFT}$ is CFT output torque.

The CFT transmission is designed to transfer energy into and out of the flywheel in a controlled manner through a slipping clutch. The CFT uses three step-gear ratios in order to reduce slip speed between the input and output shafts of the CFT, resulting in reduced clutch losses. Figure 8 illustrates a three dimensional view of the CFT with three gear ratios. The input shaft of the CFT is directly connected to the flywheel, and the output shaft of the CFT (shown at the center of the Fig. 8) is connected to the transmission output shaft through a set of speed reduction gears.

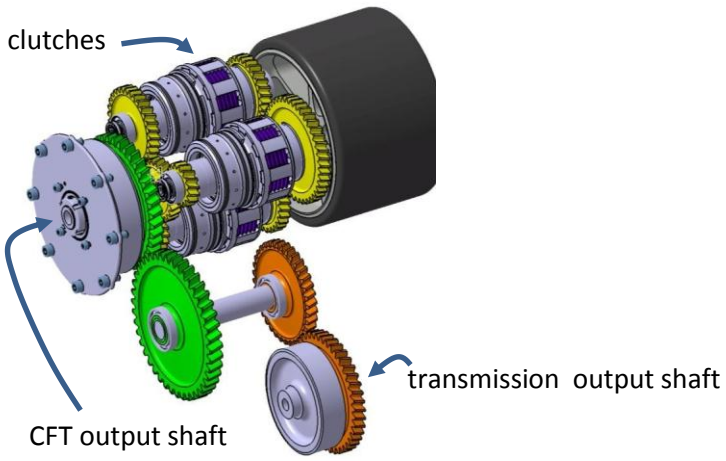

Figure 8: Three dimensional view of the CFT.

Based on the above understanding of the CFT and its operation, a CFT model and its control algorithm were developed. With the assumption of fast clutch servo-loop dynamics, the torque output of the CFT is assumed to perfectly track the requested torque signal. That is,

$$T_{o,CFT} = T_{req,CFT} \tag{9}$$

Knowing that two clutch torques on the input and output side plates are equal, the $T_{i,CFT}$ is computed as follows

$$T_{i,CFT} = \frac{T_{o,CFT}}{GR_{SR}GR_{CFT,o}GR_{CFT,i}} \quad (10)$$

where GR_{SR} is the three-stage speed reduction gear ratio, $GR_{CFT,o}$ and $GR_{CFT,i}$ are output and input side gear ratios of the slipping clutch, respectively, which is determined by the gear selection.

The clutch loss is computed as follows.

$$E_{CFT,loss} = \int T_{clutch,k}\,\Delta\omega_k dt \quad (11)$$

with k =1, 2, and 3, representing each CFT gear, $T_{clutch,k}$ is the torque across the slipping clutch k, and $\Delta\omega_k$ is the slip speed across the slipping clutch k. Thus, the clutch loss is minimized when the slip speed is minimized for a given $T_{o,CFT}$. In order to find the optimal gear that minimizes slip speed, let us define three slip speeds across three clutches as follows.

$$\Delta\omega_k = GR_{SR}GR_{o,k}\omega_{o,CFT} - \frac{\omega_{i,CFT}}{GR_{i,k}} \quad (12)$$

where $GR_{i,k}$, $GR_{o,k}$ are respectively the input and output side gear ratios of the slipping clutch, and $\omega_{i,CFT}$, $\omega_{o,CFT}$ are respectively the CFT input and output speeds.

Then, we can find which CFT mode we are in using the conditions of these three slip speeds. That is,

$$\begin{array}{cccc} & \Delta\omega_1 < 0 & \Delta\omega_1 > 0 & \Delta\omega_1 > 0 & \Delta\omega_1 > 0 \\ \text{Mode 1: } & \Delta\omega_2 < 0 & \text{Mode 2: } \Delta\omega_2 < 0 & \text{Mode 3: } \Delta\omega_2 > 0 & \text{Mode 4: } \Delta\omega_2 > 0 \\ & \Delta\omega_3 < 0 & \Delta\omega_3 < 0 & \Delta\omega_3 < 0 & \Delta\omega_3 > 0 \end{array}$$

Note that mode 1 must select gear 1 and mode 4 must select gear 3. However, mode 2 may choose gear 1 or 2 and mode 3 may choose gear 2 or 3 depending on the direction of power flow. Since the power flow can be easily determined by $T_{req,CFT}$, one can choose the optimal gear using the three slip speed conditions.

The flywheel dynamics model is described by a simple rotational inertia with two torques acting on it; one is the CFT input torque, and the other is the internal flywheel loss as Eq. (13) shows.

$$\frac{d\omega_f}{dt} = \frac{T_{i,CFT} + T_{f,loss}}{I_f} \quad (13)$$

where $T_{f,loss}$ represents flywheel friction and viscous losses.

The control strategy basically stores vehicle kinetic energy during braking and uses this up during the next vehicle launch. Thus, no hybrid (blending) modes are actively used during acceleration or cruising. The control algorithm is designed as follows.

If SOC > 0.01 and P_{dem} < 50 kw and V < 50mph

$E_{on/off}$ = 0

Else

$E_{on/off}$ = 1 and $P_{eng} = P_{dem}$

where P_{dem} is demanded power, $E_{on/off}$ is the engine on/off flag

6 Simulation Results and Discussion

Energy analysis shows that the warm-start urban fuel economy of the flywheel hybrid vehicle is improved significantly. The fuel economy improvement mainly comes from 1) idle stop/start, 2) recuperation of the braking energy, and 3) higher engine efficiency by launching the vehicle with the flywheel. Fig. 9 illustrates that braking energy has been reduced due to regenerative braking via kinetic energy recuperation, but this gain is partly offset by the flywheel bearing and CFT losses. The idle stop/start gain alone is 6%, with 9% attributable to items 2) and 3). Although total component losses are not significantly reduced, the elimination of the idle stop/start and low-efficiency engine operation during deceleration and launch results in significant fuel economy improvement.

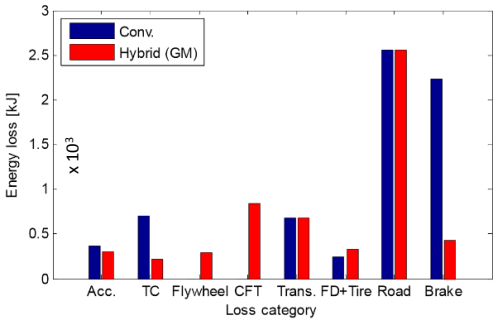

Figure 9: Fuel Economy and Energy Analysis of the Simulation Results over the FTP Urban Drive Cycle.

By examining the time response of the flywheel hybrid vehicle simulation results, we obtained a good understanding of how the engine and flywheel are operated

throughout the drive cycle. Note that, unlike hybrid electric vehicles, the SOC starts at 0 and stays low throughout the drive cycle because the flywheel is initially completely discharged and the supervisory controller is designed to recharge only during braking; this energy is completely discharged during the next vehicle launch. If launching the vehicle solely with the flywheel proves impractical, the fuel economy benefit will be reduced.

7 Summary

This paper presents two interesting mechanisms-related problems in the area of advanced propulsion systems, one in power generation and the other in power transmission. The first is an opposed-piston variable compression ratio engine mechanism for possible use in advanced powertrains. The concept is a two-stroke engine equipped with a Roots supercharger to facilitate the scavenging process. The engine has been numerically evaluated using 1-D and 3-D simulation tools. We present the kinematic details of the mechanism arrangement that serves to couple the two cranks which may be selectively phased relative to each other to achieve a variable compression ratio. Secondly, the paper describes a high-speed flywheel system and its use as an alternative energy storage system for recapturing vehicle kinetic energy as a low-cost hybrid architecture. Such a system has the potential to improve fuel economy by 15-20% on the certification drive-cycle when coupled to the driveline via a three-speed clutched transmission system in a representative mid-size vehicle. The fuel economy gain is shown to be due to idle stop/start, recuperation of vehicle kinetic energy during deceleration events, launching of the vehicle with the flywheel, and driveline torque boosting to offset fuel use. We have presented simulation results on drive cycle fuel consumption as well as the kinematic details of the geared arrangement to get energy into and out of the flywheel system.

8 References

[1] International Energy Outlook 2013, http://www.eia.gov/forecasts/archive/ieo13/pdf/0484(2013).pdf

[2] Robinette, D., and Powell, M., “Optimizing 12V Start-Stop for Conventional Powertrains,” SAE 2011-01-0699.

[3] Hawkins, S., Billotto, F., Cottrell, D., Houtman, A., Poulos, S., Rademacher, R., Van Maanen, K., and Wilson, D., “Development of General Motors’ eAssist Powertrain,” SAE Int. J. Alternative Powertrains, Volume 1, Issue 1, 2012, pp. 308-323.

[4] Schmidt, M., “Two-Mode, Compound-Split Electromechanical Vehicular Transmission,” U.S. Patent 5,931,757, August 3, 1999.

[5] Grewe, T., Conlon, B., and Holmes, A., “Defining the General Motors 2-Mode Hybrid Transmission,” SAE 2007-01-0273.

[6] Miller, M., Holmes, A., Conlon, B., and Savagian, P., “The GM Voltec 4ET50 Multi-Mode Electric Transaxle,” SAE 2011-01-0887.

[7] Conlon, B., Blohm, T., Harpster, M., Holmes, A., Palardy, M., Tarnowsky, S., and Zhou, L., “The Next Generation “Voltec” Extended Range EV Propulsion System,” SAE 2015-01-1152.

[8] Raghavan, M., Chanumolu, R., and Park, F., "Novel Propulsion and Energy Recharge Architectures for Urban Vehicles," Proceedings of EVS 28, KINTEX, Korea, May 3-6, 2015.

[9] Raghavan, M., "Propulsion Architectures using Mechanical Energy Storage," in *New Trends in Mechanism and Machine Science*, Volume 24, 2015, pp 817-825

[10] Maguire, J., Bucknor, N., Raghavan, M., and Najt, P., "Hybrid Powertrain," US Patent 7611432, 3 Nov, 2009.

[11] Wright, P., F1 moves toward hybridization, Automotive Engineering International, pp. 60-63, May 2008.

[12] Hebner, R., J. Beno, and A. Walls, Flywheel batteries come around again, IEEE Spectrum April 2002, pp. 46-51.